

Interplay between excitation kinetics and reaction-center dynamics in purple bacteria

Felipe Caycedo-Soler, Ferney J. Rodríguez and Luis Quiroga

Departamento de Física, Universidad de Los Andes, A.A. 4976 Bogotá, D.C., Colombia

Neil F. Johnson

Department of Physics, University of Miami, Coral Gables, Miami, Florida 33126, USA

E-mail: f-cayced@uniandes.edu.co

Abstract. Photosynthesis is arguably the fundamental process of Life, since it enables energy from the Sun to enter the food-chain on Earth. It is a remarkable non-equilibrium process in which photons are converted to many-body excitations which traverse a complex biomolecular membrane, getting captured and fueling chemical reactions within a reaction-center in order to produce nutrients. The precise nature of these dynamical processes – which lie at the interface between quantum and classical behaviour, and involve both noise and coordination – are still being explored. Here we focus on a striking recent empirical finding concerning an illumination-driven transition in the biomolecular membrane architecture of *Rsp. Photometricum* purple bacteria. Using stochastic realisations to describe a hopping rate model for excitation transfer, we show numerically and analytically that this surprising shift in preferred architectures can be traced to the interplay between the excitation kinetics and the reaction center dynamics. The net effect is that the bacteria profit from efficient metabolism at low illumination intensities while using dissipation to avoid an oversupply of energy at high illumination intensities.

1. Introduction

In addition to its intrinsic interest as one of Nature's oldest and most important processes, photo-energy conversion is of great practical interest given Society's pressing need to reduce reliance on fossil fuels by exploiting alternative energy production. Photosynthesis maintains the planet's oxygen and carbon cycles in equilibrium [1, 2, 3] and efficiently converts sunlight [4, 5, 6], while the possibility of its *in vivo* study provides a fascinating window into the aggregate effect of millions of years of natural selection. Among the most widespread photosynthetic systems are purple bacteria *Rsp. Photometricum* which manage to sustain their metabolism even under dim light conditions within ponds, lagoons and streams [7]. They absorb light through antenna structures in the biomolecular Light Harvesting complex 2 (LH2), and transfer the electronic excitation along the membrane to Light Harvesting complexes 1 (LH1) which each contain a Reaction Center (RC) complex. If charge carriers are available (i.e. the RC is in an open state), then the resulting reactions will feed the bacterial metabolism.

It was recently observed [1] that the photosynthetic membranes in *Rsp. Photometricum* adapt to the light intensity conditions under which they grow. Illuminated under High Light Intensity (HLI) ($I_0 \approx 100\text{W/m}^2$ where I_0 is the growing light intensity), membranes grow with a ratio of antenna-core complexes (i.e. stoichiometry) $\text{LH2/LH1} \approx 3.5\text{-}4$. For Low Light Intensity (LLI) ($I_0 \approx 10\text{W/m}^2$), this ratio increases to 7-9. The features that reveal an unexpected change in the ratio of harvesting complexes, in bacterias grown under HLI and LLI are shown in Fig.1(a) and Fig.1(b), respectively. Here we present a quantitative theory to explain this adaptation in terms of a dynamical interplay between excitation kinetics and reaction-center dynamics. In particular, the paper lays out the model, its motivation and implications, in a progressive manner in order to facilitate understanding. Although our model treats the excitation transport as a noisy, classical process, we stress that the underlying quantities being transported are quantum mechanical many-body excitations [8, 9]. The membrane architecture effectively acts as a background network which loosely coordinates the entire process.

2. Structure of complexes and excitation kinetics in small networks

Figure 2 summarizes the relevant biomolecular complexes in purple bacteria *Rsp. Photometricum* [10], together with timescales governing the excitation kinetics and reaction center dynamics. Each LH2 can absorb light with wavelengths 839 to 846 nm, while LH1 absorbs maximally at 883 nm. The LH1 forms an ellipse which completely surrounds the reaction center (RC) complex. Within the RC, a dimer of bacteriochlorophylls (BChls) known as the special pair P, can be excited. The excitation (P^*) induces ionization (P^+) of the special pair, and hence metabolism. The initial photon absorption is proportional to the complex cross-sections, which have been calculated for LH1 and LH2 complexes [11]. With $n(\lambda)$ incident photons of wavelength λ , an

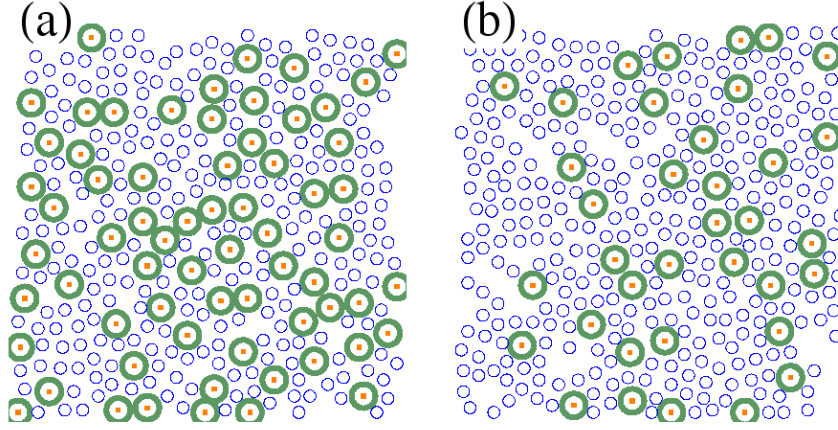


Figure 1. Empirical architectures for (a) HLI and (b) LLI membranes, displaying LH2s (small blue circles), LH1s (big green circles) and RCs (orange dots).

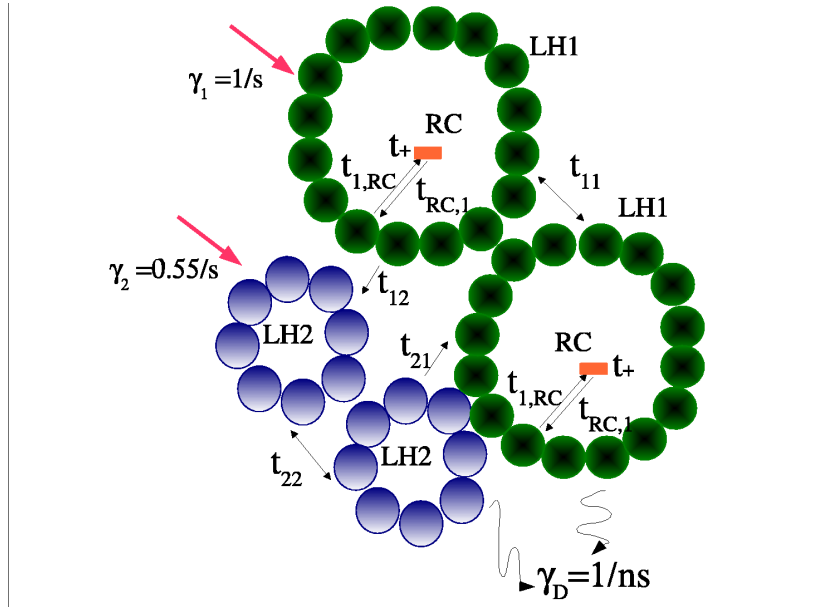


Figure 2. Schematic of the biomolecular photosynthetic machinery in purple bacteria, together with relevant inter-complex mean transfer times t_{ij} , dissipation rate γ_D , and normalized light intensity rate $\gamma_{1(2)}$

18 W/m² light intensity yields a photon absorption rate for circular LH1 complexes in *Rb. sphaeroides* [12] given by $\int n(\lambda)\sigma_{\text{LH1}}(\lambda)d\lambda = 18\text{s}^{-1}$, where σ_{LH1} is the LH1 absorption cross section. For LH2 complexes, the corresponding photon capture rate is 10s⁻¹. Extension to other intensity regimes is straightforward, by normalizing to unit light intensity. The rate of photon absorption normalized to 1 W/m² intensity, will be $\gamma_1 = \frac{18}{18} = 1\text{s}^{-1}$ for an individual LH1, and $\gamma_2 = \frac{10}{18} = 0.55\text{s}^{-1}$ for individual LH2 complexes. The complete vesicle containing several hundreds of complexes, will have an absorption rate $\gamma_A = I(\gamma_1 N_1 + \gamma_2 N_2)$ where $N_{1(2)}$ is the number of LH1 (LH2) complexes

in the vesicle, and I is the light intensity. The number of RC complexes is therefore also equal to N_1 . Excitation transfer occurs through induced dipole transfer, among BChls singlet transitions. The common inter-complex BChl distances 20-100 Å [1, 13] cause excitation transfer to arise through the Coulomb interaction on the picosecond time-scale [14], while vibrational dephasing destroys coherences within a few hundred femtoseconds [15, 16]. The Coulomb interaction de-excites an initially excited electron in the donor complex while simultaneously exciting an electron in the acceptor complex. As dephasing occurs, the donor and acceptor phase become uncorrelated. Transfer rate measures from pump-probe experiments agree with generalized Förster calculated rates [14], assuming intra-complex delocalization. LH2→LH2 transfer has not been measured experimentally, although an estimate of $t_{22} = 10$ ps has been calculated [14]. LH2→LH1 transfer has been measured for *R. Sphaeroides* as $t_{21} = 3.3$ ps [17]. Due to formation of excitonic states [8, 9], back-transfer LH1→LH2 is enhanced as compared to the canonical equilibrium rate for a two-level system, up to a value of $t_{12} = 15.5$ ps. The LH1→LH1 mean transfer time t_{11} has not been measured, but generalized Förster calculation [18] has reported an estimated mean time t_{11} of 20 ps. LH1→RC transfer occurs due to ring symmetry breaking through second and third lowest exciton lying states [19], as suggested by agreement with the experimental transfer time of 35-37 ps at 77 K [20, 21]. Increased spectral overlap at room temperature improves the transfer time to $t_{1,RC} = 25$ ps as proposed by [22]. A photo-protective design makes the back-transfer from an RC's fully populated lowest exciton state to higher-lying LH1 states occur in a calculated time of $t_{RC,1} = 8.1$ ps [19], close to the experimentally measured 7-9 ps estimated from decay kinetics after RC excitation [23]. The first electron transfer step $P^* \rightarrow P^+$ occurs in the RC within $t_+ = 3$ ps, used for quinol (Q_BH_2) production [14]. Fluorescence, inter-system crossing, internal conversion and further dissipation mechanisms, have been included within an effective single lifetime $1/\gamma_D$ of 1 ns [18]. Due to the small absorption rates in γ_A , two excitations will only rarely occupy a single harvesting structure – hence it is sufficient to include the ground $s = 0$ and one exciton states $s = 1$ for each harvesting complex.

We now introduce the theoretical framework that we use to describe the excitation transfer, built around the experimental and theoretical parameters just outlined. In the first part of the paper, our calculations are all numerical – however we turn to an analytic treatment in the latter part of the paper. We start by considering a collective state with $N = N_2 + 2N_1$ sites – resulting from N_1 LH1s, N_2 LH2s and hence N_1 RC complexes in the vesicle – in terms of a set of states having the form $\{s_1, \dots, s_N\}$ in which any complex can be excited or unexcited, and a maximum of N excitations can exist in the membrane. If only excitation kinetics are of interest, and only two states (i.e. excited and unexcited) per complex are assumed, the set of possible states has 2^N elements. We introduce a vector $\vec{\rho} = (\rho_1, \rho_2, \dots, \rho_{2^N})$ in which each element describes the probability of occupation of a collective state comprising several excitations. Its time

evolution obeys a master equation

$$\partial_t \rho_i(t) = \sum_{j=1}^{2^N} G_{i,j} \rho_j(t). \quad (1)$$

Here $G_{i,j}$ is the transition rate from a site i to a site j . Since the transfer rates do not depend on time, this yields a formal solution $\vec{\rho}(t) = e^{\tilde{G}t} \vec{\rho}(0)$. Small absorption rates lead to single excitation dynamics in the whole membrane, reducing the size of $\vec{\rho}(t)$ to the total number of sites N . The probability to have one excitation at a given complex initially, is proportional to its absorption cross section, and can be written as $\vec{\rho}(0) = \frac{1}{\gamma_A} (\underbrace{\gamma_1, \dots}_{N_1}, \underbrace{\gamma_2, \dots}_{N_2}, \underbrace{0, \dots}_{N_1})$, where subsets correspond to the N_1 LH1s, the N_2 LH2s and the N_1 RCs respectively. Our interest lies in \hat{p}_k which is the normalized probability to find an excitation at a complex, given that at least one excitation resides in the network:

$$\hat{p}_k(t) = \frac{\rho_k(t)}{\sum_{i=1}^N \rho_i(t)}. \quad (2)$$

In order to appreciate the effects that network architecture might have on the model's dynamics, we start our analysis by studying different arrangements of complexes in small model networks, focusing on architectures which have the same amount of LH1, LH2 and RCs as shown in the top panel of Fig.3(a), (b) and (c). The bottom panel Fig.3 (d)-(f) shows that \hat{p}_k values for RC, LH1 and LH2 complexes, respectively. Fig.3(d) shows that the highest RC population is obtained in configuration (c), followed by configuration (a) and (b) whose ordering relies in the connectedness of LH1s to antenna complexes. Clustering of LH1s will limit the number of links to LH2 complexes, and reduce the probability of RC ionization. For completeness, the probability of occupation in LH1 and LH2 complexes (Figs.3(e) and (f), respectively), shows that increased RC occupation benefits from population imbalance between LH1 enhancement and LH2 reduction. As connections among antenna complexes become more favored, the probability of finding an excitation on antenna complexes will become smaller, while the probability of finding excitations in RCs is enhanced.

This discussion of simple network architectures, provides us with a simple platform for testing the notion of energy funneling, which is a phenomenon that is commonly claimed to arise in such photosynthetic structures. We start with a minimal configuration corresponding to a basic photosynthetic unit: one LH2, one LH1 and its RC. Figure 4(a) shows that excitations will mostly be found in the LH1 complex, followed by occurrences at the LH2 and lastly at the RC. Figure 4(b) shows clearly the different excitation kinetics which arise when the RC is initially unable to start the electron transfer $P^* \rightarrow P^+$, and then after ≈ 15 ps the RC population increases with respect to the LH2's. This confirms that the energy funneling concept is valid for these small networks [14, 18], i.e. excitations have a preference to visit the RC ($t_{1,RC} = 25$ ps) as compared to being transferred to the light-harvesting complexes ($t_{12} = 15.5$ ps). However, in natural scenarios involving entire chromatophores with many complexes, we will show that energy funneling is not as important due to increased number of available states, provided from all LH2s surrounding a core complex.

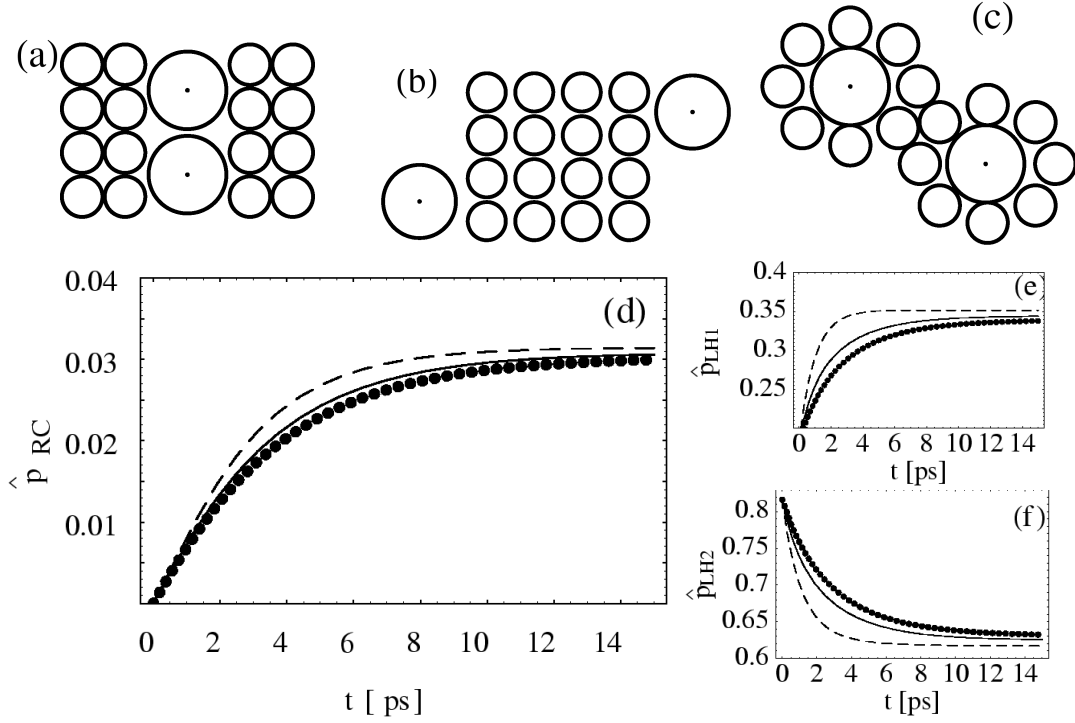


Figure 3. Top panel: Three example small network architectures. The bottom panel shows the normalized probabilities for finding an excitation at an RC (see (d)), an LH1 (see (e)), or an LH2 (see (f)). In panels (d)-(f), we represent these architectures as follows: (a) is a continuous line; (b) is a dotted line; (c) is a dashed line.

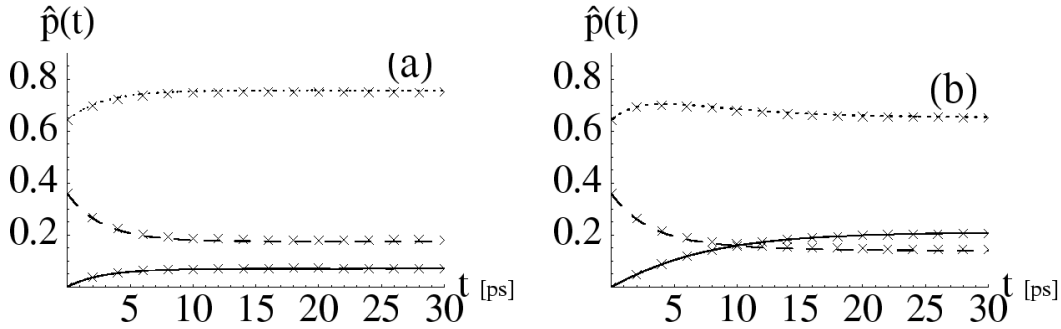


Figure 4. Normalized probabilities \hat{p}_k for finding the excitation at an LH2 (dashed), LH1 (dotted) or at an RC (continuous), for (a) $t_+ = 3$ ps, and (b) $t_+ \rightarrow \infty$. Crosses are the results from the Monte Carlo simulation.

Given the large state-space associated with such multiple complexes, our subsequent model analysis will be based on a discrete-time random walk for excitation hopping between neighboring complexes. In particular, we use a Monte Carlo method to simulate the events of excitation transfer, the photon absorption and dissipation, and the RC electron transfer. We have checked that our Monte Carlo simulations accurately reproduce the results of the population-based calculations described above, as can be seen from Figs.4(a) and (b).

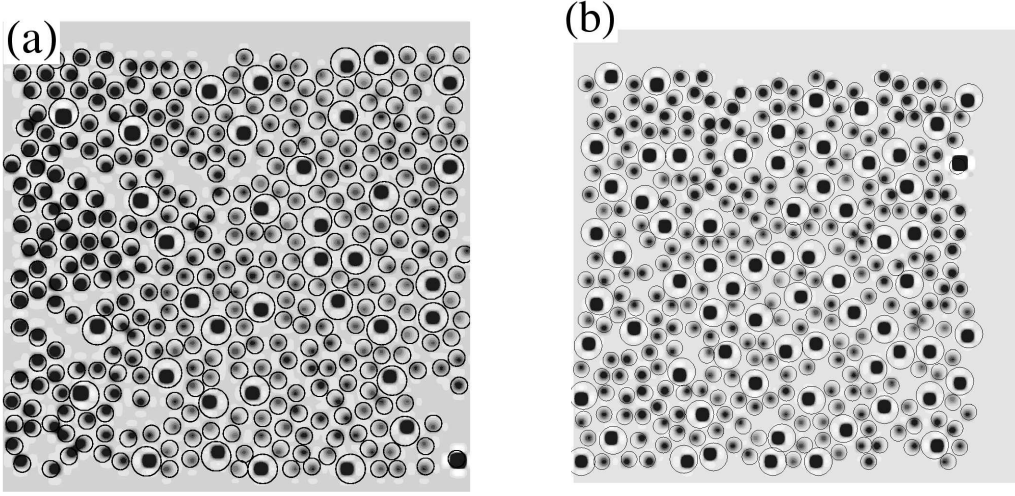


Figure 5. Contour plots for dissipation in LLI (a) and HLI (b) membranes. Greater contrast means higher values for dissipation. The simulation is shown after 10^6 excitations were absorbed by the membrane with rate γ_A .

3. Performance measures of complete chromatophore vesicles

We now turn to discuss the application of the model to the empirical biological structures of interest, built from the three types of complex k (LH1, $k=1$; LH2, $k=2$; RC, $k=3$). In particular, we have carried out extensive simulations to investigate the role of the following quantities in the complete chromatophore vesicles:

- Adjacency geometry of LH1s and LH2s. The LH2s are more abundant than LH1s and both complexes tend to form clusters, while LH2s are also generally found surrounding the LH1s.
- The average time an excitation spends \hat{t}_k in complex type k .
- The probability p_{R_k} of finding an excitation in complex type k .
- Dissipation d_i which measures the probability for excitations to dissipate at site i , from which the probability D_k of dissipation in core or antenna complexes can be obtained by adding all d_i concerning complex type k .
- The sum over all complexes of the dissipation probability, which gives the probability for an excitation to be dissipated. The efficiency of the membrane is the probability of using an excitation in any RC, i.e. $\eta = 1 - \sum_i d_i$.

Figure 5(a) shows that the membrane grown under low light intensity (LLI) has highly dissipative clusters of LH2s, in contrast to the uniform dissipation in the high light intensity (HLI) membrane (see Fig.5(b)). This result is supported by a tendency for excitations to reside longer in LH2 complexes far from core centers (not shown), justifying the view of LH2 clusters as excitation reservoirs. However, for LLI and HLI, the dissipation in LH1 complexes is undistinguishable. In Table 1 we show the observables obtained using our numerical simulations. These show that:

(i) Funneling of excitations:

- The widely held view of the funneling of excitations to LH1 complexes, turns out to be a small network effect, which by no means reflects the behavior over the complete chromatophore. Instead, we find that excitations are found residing mostly in LH2 complexes.
- Since a few LH2s surround each LH1, the mean residence times t_k in all complexes is very similar.

(ii) Dissipation and performance:

- Excitations are dissipated more efficiently in individual LH1 complexes, since $\frac{D_1}{N_1} > \frac{D_2}{N_2}$.
- Dissipation in a given complex type depends primarily on its relative abundance, since $\frac{D_k}{D_j} \approx \frac{N_k}{N_j}$
- HLI membranes are more efficient than LLI membranes.

Membrane	\hat{t}_2	\hat{t}_1	p_{R_2}	p_{R_1}	D_2	D_1	$\frac{D_2}{N_2}$	$\frac{D_1}{N_1}$	$\frac{D_2}{D_1}$	$s = \frac{N_2}{N_1}$	$\eta = \frac{n_{RC}}{n_A}$
LLI	2.22	2.39	0.72	0.25	0.74	0.26	2.2	7.2	9.13	9.13	0.86
HLI	1.70	2.65	0.50	0.46	0.52	0.48	1.9	7.1	3.88	3.92	0.91

Table 1. Residence time \hat{t}_k (in picoseconds), dissipation D_k , residence probability p_{R_k} , unitary dissipation per complex $\frac{D_k}{N_k}$ ($\times 10^{-3}$), on $k = \{1, 2\}$ corresponding to N_1 LH1 and N_2 LH2 complexes respectively. Stoichiometry s and efficiency η are also shown.

For the present discussion, the most important finding from our simulations is that the adaptation of purple bacteria does *not* lie in the single excitation kinetics. In particular, LLI membranes are seen to reduce their efficiency globally at the point where photons are becoming scarcer – hence the answer to adaptation must lie in some more fundamental trade-off (as we will later show explicitly). Due to the dissimilar timescales between millisecond absorption [12] and nanosecond dissipation [14], multiple excitation dynamics are also unlikely to occur within a membrane. However we note that simulations involving multiple excitations, that include blockade (Fig.6(a)) in which two excitations can not occupy the same site, does not appreciably lower the efficiency η up to thirty excitations. We find that annihilation (Fig.6(b)), in which two excitations annihilate when they occupy the site at the same time, diminishes the membrane’s performance equally in both HLI and LLI membranes.

Our findings above show that the explanation for the observed architecture adaptations (HLI and LLI) neither lies in the frequently quoted side-effect of multiple excitations, nor in the excitation dynamics alone. Instead, as we now explain, the answer as to how adaptation can prefer the empirically observed HLI and LLI structures under different illumination conditions, lies in the *interplay* between the excitation kinetics and reaction-center cycling dynamics. By virtue of quinones-quinol and cytochrome charge carriers, the RC dynamics features a ‘dead’ (or equivalently ‘busy’) time interval during

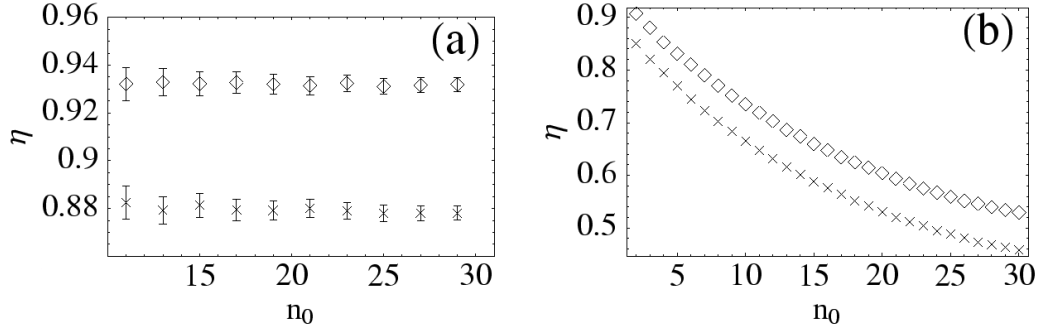


Figure 6. Efficiency of multiple excitation dynamics: (a) blockade and (b) annihilation mechanisms, for LLI (crosses) and HLI (diamonds) membranes. n_0 corresponds to the initial number of excitations in each realization.

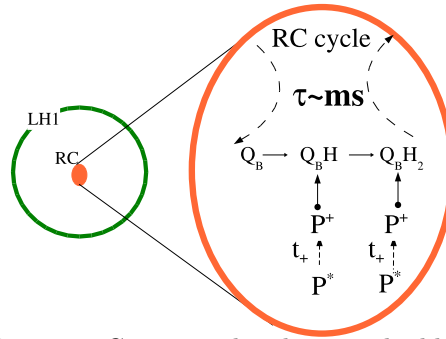


Figure 7. Reaction Center cycle, showing double reduction of the special pair P together with formation of quinol $Q_B H_2$. There is a dead time τ on the millisecond time-scale, before a new quinone Q_B becomes available.

which quinol is produced, removed and then a new quinone becomes available [24, 25]. A single oxidation $P^* \rightarrow P^+$ will produce $Q_B H$ in the reaction $Q_B \rightarrow Q_B^- \rightarrow Q_B H$, and a second oxidation will produce quinol $Q_B H_2$ in the reaction $Q_B H \rightarrow Q_B H^- \rightarrow Q_B H_2$. Once quinol is produced, it leaves the RC and a new quinone becomes attached. The cycle is depicted in Fig. 7, and is described in the simulation algorithm by closing an RC for a time τ after two excitations form quinol. This RC cycling time τ implies that at any given time, not all RCs are available for turning the electronic excitation into a useful charge separation. Therefore, the number of useful RCs decreases with increasing τ . Too many excitations will rapidly close RCs, implying that any subsequently available nearby excitation will tend to wander along the membrane and eventually be dissipated - hence reducing η . For the configurations resembling the empirical architectures (Fig.1), this effect is shown as a function of τ in Fig. 8(a) yielding a wide range of RC-cycling times at which LLI membrane is more efficient than HLI. Interestingly, this range corresponds to the measured time-scale for τ of milliseconds [24, 25], and supports the suggestion that bacteria improve their performance in LLI conditions by enhancing quinone-quinol charge carrier dynamics as opposed to manipulating exciton transfer. A recent proposal [27] has shown numerically that the formation of LH2 para-crystalline domains produces a clustering trend of LH1 complexes with enhanced quinone availability - a fact that

would reduce the RC cycling time. However, the crossover of efficiency at $\tau \approx 3$ ms implies that even if no enhanced RC-cycling occurs, the HLI will be less efficient than the LLI membranes on the observed τ time-scale. The explanation is quantitatively related to the number N_o of open RCs. Figs. 8(b), (c) and (d) present the distribution $p(N_o)$ of open RCs, for both HLI and LLI membranes and for the times shown with arrows in Fig.8(a). When the RC-cycling is of no importance (Fig. 8(b)) almost all RCs remain open, thereby making the HLI membrane more efficient than LLI since having more (open) RCs induces a higher probability for special pair oxidation. Near the crossover in Fig. 8, both membranes have distributions $p(N_o)$ centered around the same value (Fig. 8(c)), indicating that although more RCs are present in HLI vesicles, they are more frequently closed due to the ten fold light intensity difference, as compared to LLI conditions. Higher values of τ (Fig. 8(d)) present distributions where the LLI has more open RCs, in order to yield a better performance when photons are scarcer. Note that distributions become wider when RC cycling is increased, reflecting the mean-variance correspondance of Poissonian statistics used for simulation of τ . Therefore the trade-off between RC-cycling, the actual number of RCs and the light intensity, determines the number of open RCs and hence the performance of a given photosynthetic vesicle architecture (i.e. HLI versus LLI). Guided by the Monte Carlo numerical results, we develop in Sec. 5 an analytical model (continuous lines in Fig.8) that supports this discussion.

For completeness, we now quantify the effect of incident light intensity variations relative to the light intensity during growth, with both membranes having $\tau = 3$ ms. The externally applied light intensity I/I_0 , which corresponds to the ratio between the actual (I) and growth (I_0) light intensities, is varied in Fig. 9(a). The LLI membrane performance starts to diminish well beyond the growth light intensity, while the HLI adaptation starts diminishing just above I_0 due to increased dissipation. The crossover in efficiency at $I \approx I_0$ results from the quite different behaviors of the membranes as the light intensity increases. In particular, in LLI membranes excess photons are readily used for bacterial metabolism, and HLI membranes exploit dissipation in order to limit the number of processed excitations. Figs. 9(b), (c) and (d) verify that performance of membranes heavily depends on the number of open RCs. For instance, membranes subject to low excitation intensity (Fig. 9(b)) behave similarly to that expected for fast RC cycling times (Fig. 8(a)). The complete distributions, both for HLI and LLI conditions, shift to lower N_o with increased intensity in the same manner as that observed with τ . Even though these adaptations show such distinct features in the experimentally relevant regimes for the RC-cycling time and illumination intensity magnitude [1, 24, 25], Figs.8(c) and (d) show that the distributions of open RCs actually overlap. Despite the fact that the adaptations arise under different environmental conditions, the resulting dynamics of the membranes are quite similar. Note that within this parameter subspace of I and τ , the LLI membrane may have a larger number of open RCs than the HLI adaptation. In such a case, the LLI membrane will perform better than HLI with respect to RC ionization. The inclusion of RC dynamics implies

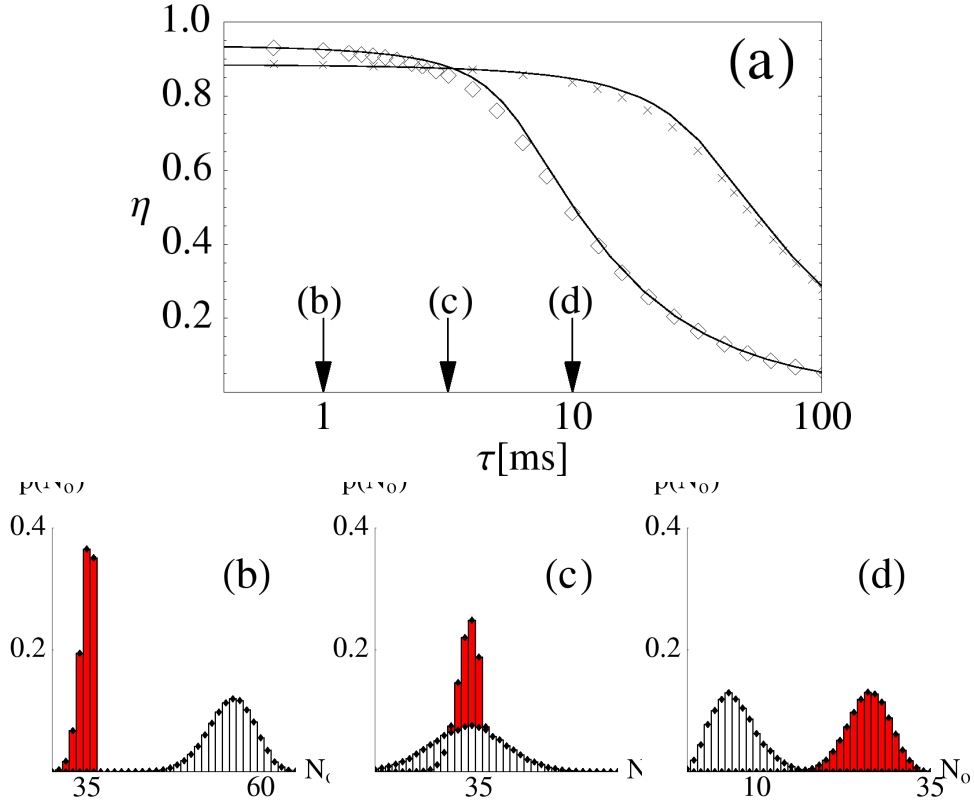


Figure 8. (a) Monte Carlo calculation of efficiency η of HLI (diamonds) and LLI (crosses) grown membranes, as a function of the RC-cycling time τ . Continuous lines give the result of the analytical model. (b), (c) and (d) show the distributions $p(N_o)$ of the number of open RCs for the times shown with arrows in the main plot for HLI (filled bars) and LLI (white bars).

that the absorbed excitation will not find all RCs available. Instead, a given amount of closed RCs will eventually alter the excitation's fate since probable states of oxidation are readily reduced. In a given lifetime, an excitation will find (depending on τ and I) a number of available RCs – which we refer to as *effective stoichiometry* – which is different from the actual number reported by Atomic Force Microscopy [1, 13].

4. Clustering trends

The empirical AFM investigations show two main features which highlight the architectural change in the membrane as a result of purple bacteria's adaptation: the stoichiometry variation and the trend in clustering. Fig. 10 shows the importance of the arrangement of complexes by comparing architectures (b), (c), (d) and (e), all of which have a stoichiometry which is consistent with LLI vesicles. Fig. 10(a) shows the difference between a given membrane's efficiency η , and the mean of all the membranes $\bar{\eta}$, i.e. $\Delta\eta = \eta - \bar{\eta}$. The more clustered the RCs, the lower the efficiency in the short τ domain. As RC cycling is increased, (b) becomes the least efficient while all other configurations perform almost equally. The explanation comes from the importance

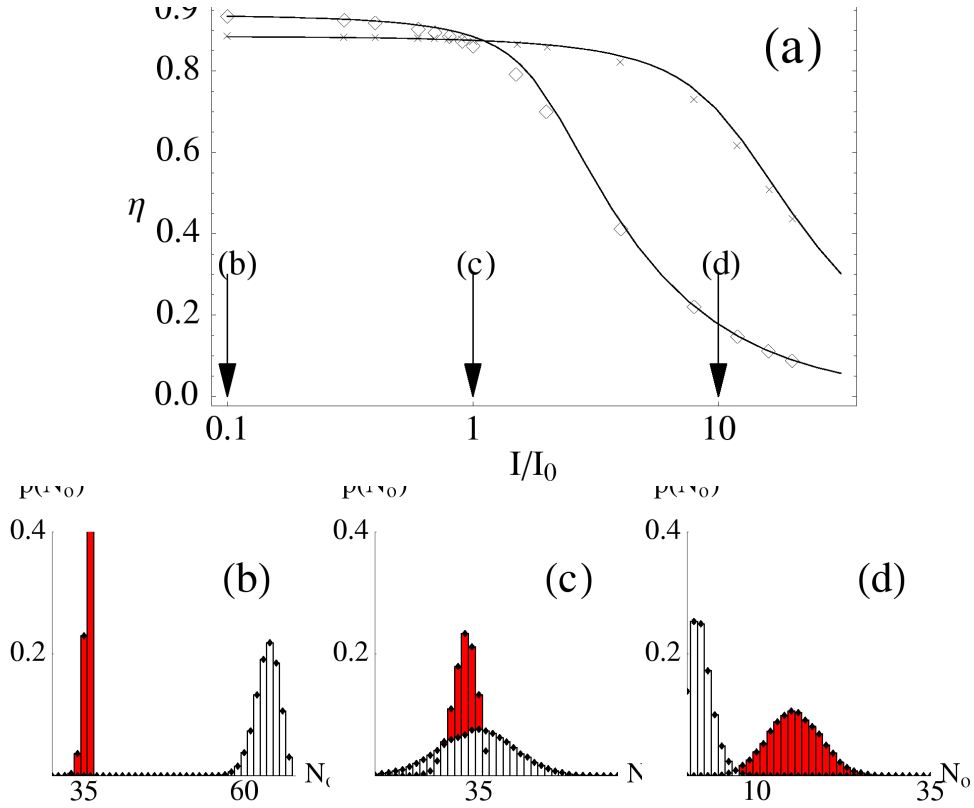


Figure 9. (a) Results from our Monte Carlo calculation of efficiency η of HLI (diamonds, $I_0 = 100 \text{ W/m}^2$) and LLI (crosses, $I_0 = 10 \text{ W/m}^2$) membranes, as a function of incident light intensity I/I_0 . Continuous lines give the result of the analytical model. Panels (b), (c) and (d) show the distribution $p(N_o)$ of the number of open RCs for light intensities corresponding to arrows in the main plot. HLI are shaded bars and LLI are white bars.

of the number of open RCs: As τ gets larger, many RCs will close and the situation becomes critical at $\tau \approx 3 \text{ ms}$, where η decreases rapidly. Configurations (c), (d) and (e) all have the same number of RCs (i.e. 44), and the distribution of open RCs is almost the same in each case for any fixed RC cycling time. By contrast, (b) has fewer RCs (i.e. 36). Therefore when τ is small, sparser RCs and exciton kinetics imply that the membrane architecture (b) will have better efficiency than (c) and (e). The effect of the arrangement itself is lost due to slower RC dynamics, and the figure of merit that determines efficiency is the number of open RCs, which is lower for (b).

To summarize so far, we find that the arrangement of complexes changes slightly the efficiency of the membranes when no RC dynamics is included – but with RC dynamics, the most important feature is the number of open RCs which is smaller for (b). The nearly equal efficiency over the millisecond τ domain, emphasizes the relative insensitivity to the complexes' geometrical arrangement. The slower the RC cycling, the more evenly available RCs will be dispersed in clustered configurations, resembling the behavior of sparse RC membranes. Incoming excitations in clustered configurations may quickly reach a cluster bordering closed RCs, but must then explore further in order to

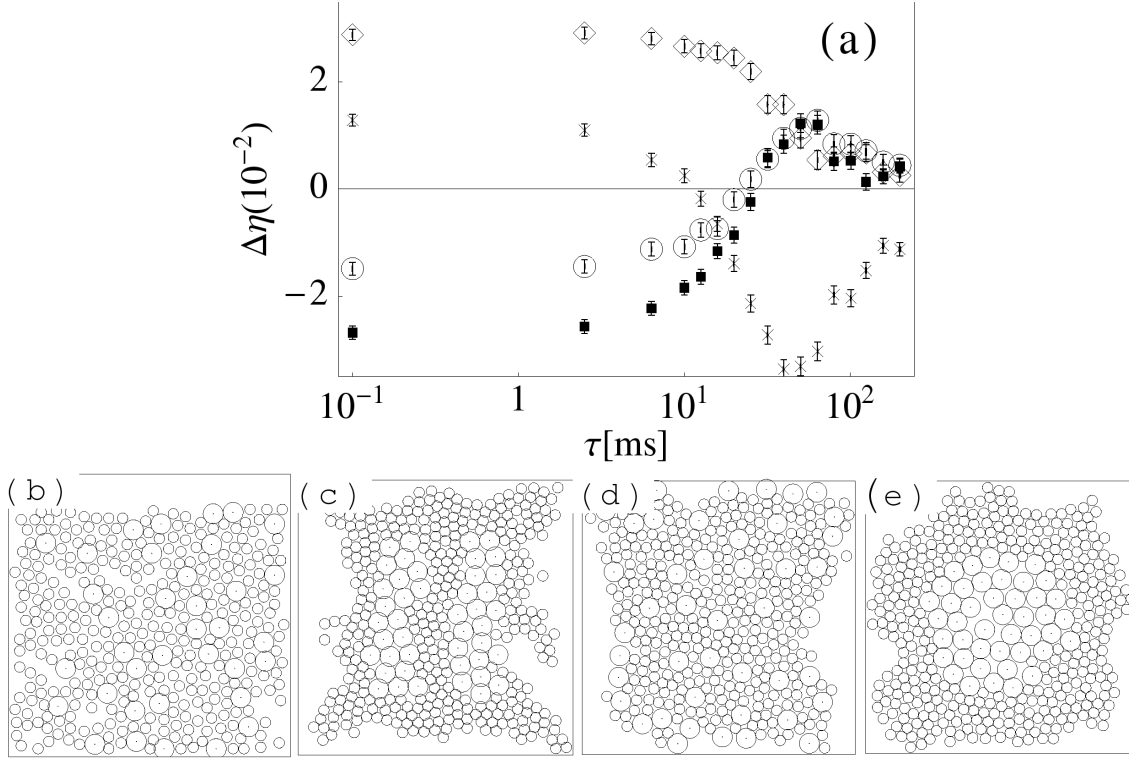


Figure 10. (a) $\Delta\eta$ is presented for the following membrane configurations: (b) *Rsp. Photometricum* bacteria; (c) *Rs. Palustris* bacteria; (d) completely unclustered vesicle; (e) fully clustered vesicle. The symbols are crosses, circles, diamonds and boxes, respectively

generate a charge separation. Although the longer RC closing times make membranes more prone to dissipation and decreased efficiency, it also makes the architecture less relevant for the overall dynamics. *The relevant network architecture instead becomes the dynamical one including sparse open RCs, not the static geometrical one involving the actual clustered RCs.* The inner RCs in clusters are able to accept excitations as cycling times increase, and hence the RCs overall are used more evenly. This implies that there is little effect of the actual configuration, and explains the closeness of efficiencies for different arrangements in the millisecond range.

5. Global membrane model incorporating excitation kinetics and RC-cycling

Within a typical fluorescence lifetime of 1 ns, a single excitation has travelled hundreds of sites and explored the available RCs globally. The actual arrangement or architecture of the complexes seems not to influence the excitation's fate, since the light intensity and RC cycling determine the number of open RCs and the availability for P oxidation. This implies that the full numerical analysis of the excitation kinetics, while technically more accurate, may represent excessive computational effort – either due to the size of

the state space within the master equation approach, or the number of runs required for ensemble averages with the stochastic method. In addition, within neither numerical approach is it possible to deduce the direct functional dependence of the efficiency on the parameters describing the underlying processes. To address these issues, we present here an alternative rate model which is inspired by the findings of the numerical simulations, but which (1) globally describes the excitation dynamics and RC cycling, (2) leads to analytical expressions for the efficiency of the membrane and the rate of quinol production, and (3) sheds light on the trade-off between RC-cycling and exciton dynamics [26].

We start with the observation that absorbed excitations are transferred to RCs, and finally ionize special pairs or are dissipated. At any given time N_E excitations will be present in the membrane. The rate at which they are absorbed is γ_A . Excitations reduce quinone Q_B in the membrane at RCs due to P oxidation at a rate $\lambda_C N_E$, or dissipate at a rate $\gamma_D N_E$. Both processes imply that excitations leave the membrane at a rate $\frac{dN_E}{dt} = -\lambda_C N_E - \gamma_D N_E$. Here λ_C is the inverse of the mean time τ_{RC} at which an excitation yields a charge separation at RCs when starting from any given complex, and it depends on the current number of open RCs given by N_o . The RC cycling dynamics depend on the rate at which RCs close, i.e. $-\frac{\lambda_C(N_o)}{2} N_E$ where the $1/2$ factor accounts for the need for two excitations to produce quinol and close the RC. The RCs open at a rate $1/\tau$, proportional to the current number of closed RCs given by $N_1 - N_o$. Hence the RC-excitation dynamics can be represented by two nonlinear coupled differential equations:

$$\frac{dN_E}{dt} = -(\lambda_C(N_o) + \gamma_D)N_E + \gamma_A \quad (3)$$

$$\frac{dN_o}{dt} = \frac{1}{\tau}(N_1 - N_o) - \frac{\lambda_C(N_o)}{2} N_E. \quad (4)$$

In the stationary state, the number of absorbed excitations n_A in a time interval Δt and the number of excitations used to produce quinol n_{RC} , are given by

$$n_A = \gamma_A \Delta t \quad (5)$$

$$n_{RC} = \lambda_C(N_o) N_E \Delta t \quad (6)$$

yielding an expression for the steady-state efficiency $\eta = n_{RC}/n_A$:

$$\eta = \frac{\lambda_C(N_o) N_E}{\gamma_A}. \quad (7)$$

These equations can be solved in the stationary state for N_E and N_o , algebraically or numerically, if the functional dependence of $\lambda_C(N_o)$ is given. It is zero when all RCs are closed, and a maximum λ_C^0 when all are open. Making the functional dependence explicit, $\lambda_C(N_o)$, Fig. 11(a) presents the relevant functional form for HLI and LLI membranes together with a linear and a quadratic fit. The dependence on the rate of quinone reduction $\lambda_C(N_o)$ requires quantification of the number of open RCs, with a notation where the fitting parameter comprises duplets where first and second components relate to the HLI and LLI membranes being studied. Figure 11(a) shows

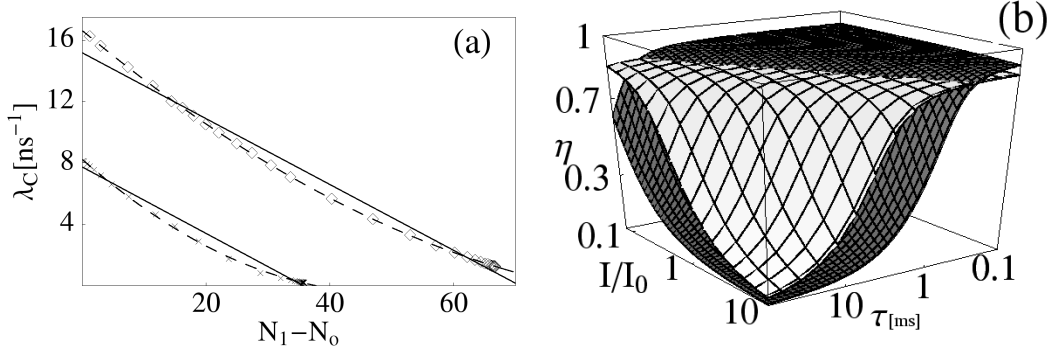


Figure 11. (a) Numerical results showing the rate of ionization $\lambda_C(N_o)$ of an RC for HLI (diamonds) and LLI (crosses) membranes, together with a quadratic (dashed line) and linear (continuous) dependence on the number of closed RCs ($N_1 - N_o$). The fitting parameters for $a + bN_o$ are $a = \{15.16, 7.72\} \text{ ns}^{-1}$, $b = \{-0.21, -0.21\} \text{ ns}^{-1}$; and for $a + bN_o + cN_o^2$, $a = \{16.61, 8.21\} \text{ ns}^{-1}$, $b = \{-0.35, -0.33\}$, and $c = \{3.6, 1.5\} \mu\text{s}^{-1}$, for HLI and LLI membranes respectively. (b) η as function of τ and $\alpha = I/I_0$, obtained from the complete analytical solution for LLI (white) and HLI (grey) membranes

that $\lambda_C(N_o)$ favors a quadratic dependence of the form $\lambda_C(N_o) = a + bN_o + cN_o^2$. A linear fit

$$\lambda_C(N_o) = \lambda_C^0 \left(\frac{N_o}{N_1} \right) \quad (8)$$

smears out the apparent power-law behavior with fit value $N_1 = \{70.72, 35.71\}$, in close agreement with the HLI and LLI membranes which have 67 and 36 RCs respectively. The linear fit $\lambda_C(N_o)$ can be used to generate an analytical expression for η as follows:

$$\eta(\tau, \gamma_A(I)) = \frac{1}{\gamma_A \lambda_C^0 \tau} \left\{ 2N_1(\lambda_C^0 + \gamma_D) + \gamma_A \lambda_C^0 \tau - \sqrt{4N_1^2(\lambda_C^0 + \gamma_D)^2 + 4N_1\gamma_A\lambda_C^0(\gamma_D - \lambda_C^0)\tau + (\gamma_A\lambda_C^0\tau)^2} \right\} \quad (9)$$

We found no analytical solution for η in the case where $\lambda_C(N_o)$ has a power law dependence. In the limit of fast RC cycling-time ($\tau \rightarrow 0$), η has the simple form $\eta = (1 + \gamma_D/\lambda_C^0)^{-1}$. If all transfer paths are summarized by λ_C^0 , this solution illustrates that $\eta \geq 0.9$ if the transfer-P reduction time is less than a tenth of the dissipation time, not including RC cycling. As can be seen in Figs. 8 and 9, the analytical solution is in good quantitative agreement with the numerical stochastic simulation, and provides support for the assumptions that we have made. Moreover, our theory shows directly that the efficiency is driven by the interplay between the RC cycling time and light intensity. Figure 11(b) shows up an entire region of parameter space where LLI membranes are better than HLI in terms of causing P ionization, even though the actual number of RCs that they have is smaller. In view of these results, it is interesting to note how clever Nature has been in tinkering with the efficiency of LLI vesicles and the dissipative behavior of HLI adaptation, in order to meet the needs of bacteria subject to the illumination conditions of the growing environment.

6. Bacterial metabolic demands: A stoichiometry prediction from our model

Photosynthetic membranes must provide enough energy to fulfill the metabolic requirements of the living bacteria. In order to quantify the quinol output of the vesicle, we calculate the quinol rate

$$W = \frac{1}{2} \frac{dn_{RC}}{dt} \quad (10)$$

which depends directly on the excitations that ionize RCs n_{RC} . The factor $\frac{1}{2}$ accounts for the requirement of two ionizations to form a single quinol molecule. Fig. 12(a) shows the quinol rate as a function of RC cycling time, when membranes are illuminated in their respective grown conditions. If RC cycling is not included ($\tau \rightarrow 0$) the tenfold quinol output difference suggests that the HLI membrane could increase the cytoplasmic pH to dangerously high levels, or that the LLI membrane could starve the bacteria. However, the bacteria manage to survive in both these conditions – and below we explain why.

In the regime of millisecond RC cycling, the quinol rate in HLI conditions decreases which is explained by dissipation enhancement acquired from only very few open RCs. Such behavior in LLI conditions appears only after several tens of milliseconds. The fact that no crossover occurs in quinol rate for these two membranes, suggests that different cycling times generate this effect. The arrows in Fig. 12(a) correspond to times where a similar quinol rate is produced in both membranes, in complete accordance with numerical studies where enhanced quinone diffusion lessens RC cycling times [27] in LLI adaptation. Although these membranes were grown under continuous illumination, the adaptations themselves are a product of millions of years of evolution. Using RC cycling times that preserve quinol rate in both adaptations, different behaviors emerge when the illumination intensity is varied (see Fig. 12). The increased illumination is readily used by the LLI adaptation, in order to profit from excess excitations in an otherwise low productivity regime. On the other hand, the HLI membrane maintains the quinone rate constant, thereby avoiding the risk of pH imbalance in the event that the light intensity suddenly increased. We stress that the number of RCs synthesized does not directly reflect the number of available states of ionization in the membrane. LLI synthesizes a small amount of RCs in order to enhance quinone diffusion, such that excess light intensity is utilized by the majority of special pairs. In HLI, the synthesis of more LH1-RC complexes slows down RC-cycling, which ensures that many of these RCs are unavailable and hence a steady quinol supply is maintained independent of any excitation increase. The very good agreement between our analytic results and the stochastic simulations, yields additional physical insight concerning the stoichiometries found experimentally in *Rsp. Photometricum*[1]. In particular, the vesicles studied repeatedly exhibit the same stoichiometries, $s \approx 4$ for HLI, and $s \approx 8$ for LLI membranes. Interestingly, neither smaller nor intermediate values are found.

We now derive an approximate expression for the quinol production rate W in terms of the environmental growth conditions and the responsiveness of purple

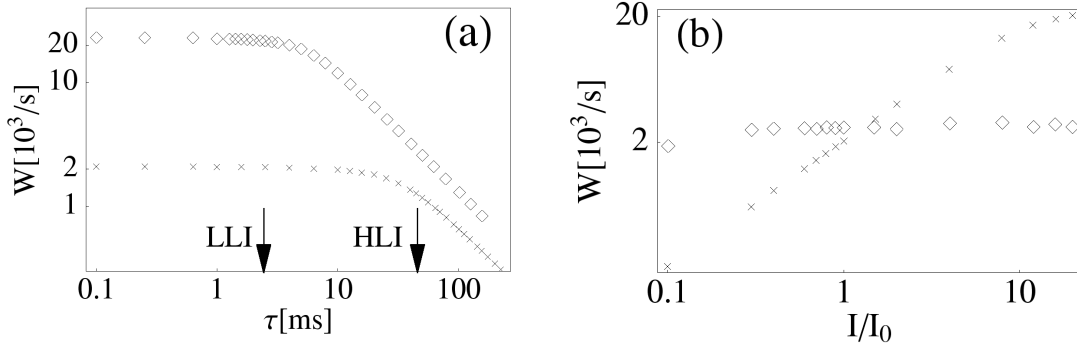


Figure 12. (a) Quinol rate W in HLI (diamonds, $I_0 = 100W/m^2$) and LLI (crosses, $I_0 = 10W/m^2$) grown membranes, as a function of RC cycling time. The times shown with arrows are used in (b), where W is presented as a function of incident intensity.

bacteria through stoichiometry adaptation. Following Refs. [1, 27, 28], the area A_0 of chromatophores in different light intensities can be assumed comparable. Initially absorption occurs with N_1 LH1 complexes of area A_1 , and N_2 LH2 complexes of area A_2 , which fill a fraction f of the total vesicle area $f = (A_1N_1 + A_2N_2)/A_0$. This surface occupancy can be rearranged in terms of the number of RCs N_1 , and the stoichiometry $N_1 = N_2/s$, yielding the expression $f = N_1(A_1 + sA_2)/A_0$. The fraction f has been shown [27] to vary among adaptations $f(s)$, since LLI have a greater occupancy than HLI membranes due to para-crystalline LH2 domains in LLI. Accordingly, the absorption rate can be cast as $\gamma_A = I(\gamma_1 + s\gamma_2)\frac{f(s)A_0}{A_1 + sA_2}$. Following photon absorption, the quinol production rate $W = \lambda_C N_E/2$ depends on the number of excitations within the membrane in the stationary state, and on the details of transfer through the rate λ_C . The assumed linear dependence $\lambda_C(N_o)$ requires knowledge of λ_C^0 and the stationary-state solution for the mean number of closed RCs through $N_o = N_1 - \frac{\lambda_C \lambda_A}{2(\gamma_D + \lambda_C)}\tau$. The stationary state in Eq. 3 yields $N_E = \frac{\lambda_A}{\gamma_D + \lambda_C}$ such that the mean number of closed RCs is simply $N_o = N_1 - W\tau$. The rate λ_C^0 is the rate at which excitations oxidize any special pair when all RCs are open. The time to reach an RC essentially depends on the number of RCs and hence the stoichiometry s . λ_C^0 must be zero when no RCs are present ($s \rightarrow \infty$) and takes a given value $\langle t_0 \rangle^{-1}$ when the membrane is made of only LH1s ($s=0$). Also the RC cycling time τ is expected to vary somewhat with adaptations due to quinone diffusion [27], which is supported in our analysis by the condition of bounded metabolic demands as presented in Fig. 12(a). The linear assumed dependence of Eq. 8 is cast explicitly as a function of W and s with the number of open RCs

$$\lambda_C(s, W) = \lambda_C^0(s) \left(1 - \frac{W\tau(s)(A_2s + A_1)}{A f(s)} \right). \quad (11)$$

From N_E in the steady state, we have

$$W = \frac{\lambda_C(s, W)\lambda_A(s, I)}{2(\lambda_C(s, W) + \gamma_D)}, \quad (12)$$

which can be solved for $W(s, I)$

$$2W(s, I) = \frac{\gamma_A(s, I)}{2} + \frac{1}{B(s)} \left(1 + \frac{\gamma_D}{\lambda_C^0} \right) + \sqrt{\left[\frac{\gamma_A(s, I)}{2} + \frac{1}{B(s)} \left(1 + \frac{\gamma_D}{\lambda_C^0} \right) \right]^2 + \frac{\gamma_A(s, I)}{2B(s)}} \quad (13)$$

where $B(s) = \frac{\tau(s)(A_1 + sA_2)}{f(s)A_0}$. To determine $\tau(s)$, we employ a linear interpolation using the values highlighted by arrows in Fig. 12(b). The requirements on $\lambda_C^0(s)$ are fulfilled by a fit $\lambda_C^0(s) = (s/a + \langle t_0 \rangle)^{-1}$, which is supported by our calculations for configurations of different stoichiometries (see Fig. 13(a)). The filling fraction $f(s)$ is assumed linear according to the experimentally found values for HLI ($f \approx 0.75$) and LLI ($f \approx 0.85$). The resulting expression is presented in Fig. 13(b). In the high stoichiometry/high intensity regime, the high excitation number would dangerously increase the cytoplasmic pH [8, 12, 14]. The contours shown in Fig. 13(c) of constant quinol production rate W , show that only in a very small intensity range will bacteria adapt with stoichiometries which are different from those experimentally observed in *Rsp. Photometricum* ($s \approx 4$ and $s \approx 8$). As emphasized in Ref. [1], membranes with $s=6$ or $s=2$ were not observed, which is consistent with our model. More generally, our results predict a great sensitivity of stoichiometry ratios for 30-40 W/m², below which membranes rapidly build up the number of antenna LH2 complexes. Very recently [29], membranes were grown with 30W/m² and an experimental stoichiometry of 4.8 was found. The contour of 2200 s⁻¹ predicts a value for stoichiometry of 4.72 at such light intensities. This agreement is quite remarkable, since a simple linear model would wrongly predict $s = 7.1$. Our theory's full range of predicted behaviors as a function of light-intensity and stoichiometry, awaits future experimental verification.

7. Concluding remarks

We have shown that excitation dynamics alone cannot explain the empirically observed adaptation of light-harvesting membranes. Instead, we have presented a quantitative model which strongly suggests that chromatic adaptation results from the interplay between excitation kinetics and RC charge carrier quinone-quinol dynamics. Specifically, the trade-off between light intensity and RC cycling dynamics induces LLI adaptation in order to efficiently promote P oxidation due to the high amount of open RCs. By contrast, the HLI membrane remains less efficient in order to provide the bacteria with a relatively steady metabolic nutrient supply.

This successful demonstration of the interplay between excitation transfer and RC trapping, highlights the important middle ground which photosynthesis seems to occupy between the fast dynamical excitation regime in which quantum-mechanical calculations are most relevant [8, 14, 30], and the purely classical regime of the millisecond timescale bottleneck in complete membranes. We hope our work will encourage further study of the implications for photosynthesis of this fascinating transition regime between quantum and classical behaviors[31]. On a more practical level, we hope that our study may help guide the design of more efficient solar micropanels mimicking natural designs.

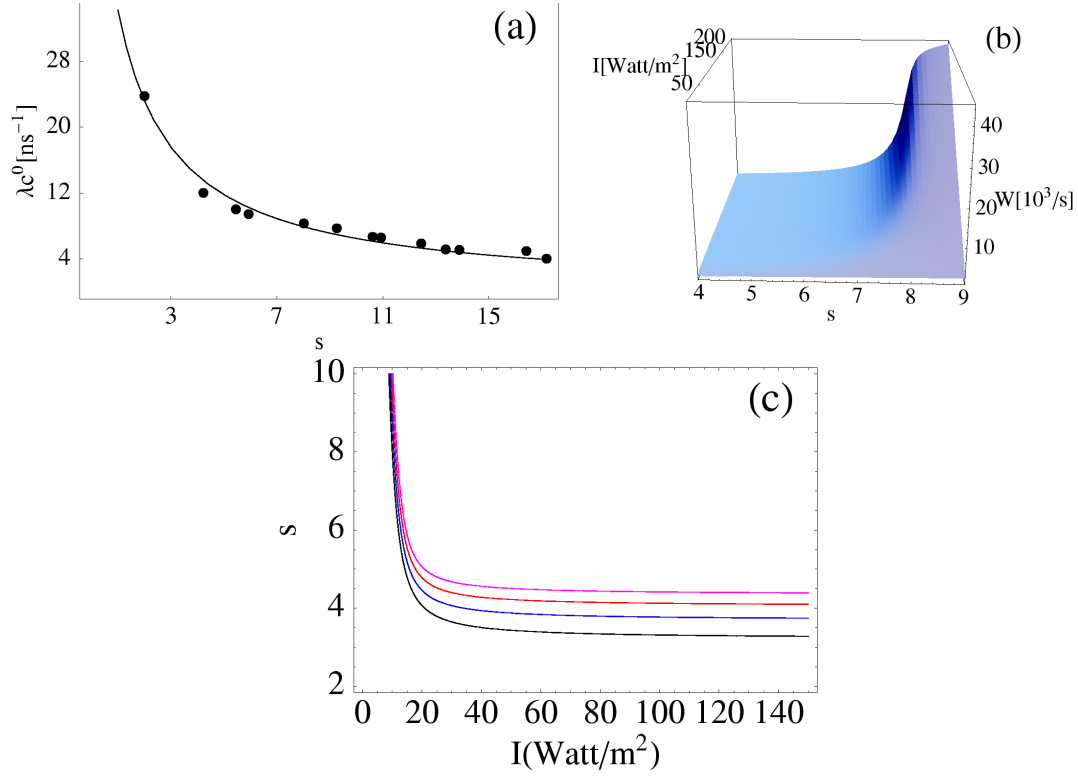


Figure 13. (a) Dependence of λ_C^0 on stoichiometry s of the membrane. (b) $W(s, I)$ as a function of stoichiometry s variation and illumination intensity. (c) Quinol rate contours of $W = \{1900, 2000, 2100, 2200\}$ s⁻¹ in black, blue, red and pink, respectively.

Aknowledgements

This research was supported by Banco de la República (Colombia) and Proyecto Semilla (2010-2011), Facultad de Ciencias Universidad de los Andes.

Appendix

Residence time t_{H_k} In the stochastic simulations, t_i^a is the residence time of an excitation in the a^{th} realization at complex i :

$$\hat{t}_k = \frac{\sum_{a, i \in k} t_i^a}{\sum_{i \in k} n_{V_i}} \quad (.1)$$

where n_{V_i} is the number of times complex i has been visited in all the stochastic realizations.

Dissipation d_i The dissipation d_i measures the probability for excitations to dissipate at site i , and can be obtained formally from

$$d_i = \frac{n_{D_i}}{n_A} \quad (.2)$$

where n_{D_i} are the number of excitations dissipated at site i and n_A is the total number of absorbed excitations.

Residence probability p_{R_k} In practice within the stochastic simulations, for a given realization a , an excitation will be a time t_1^a in LH1s, a time t_2^a in LH2s and a time t_3^a in RCs. The residence probability will become

$$p_{R_k} = \frac{\sum_a t_k^a}{\sum_{j,a} t_k^a}. \quad (.3)$$

The total time of all realizations in complex type k is the numerator, while the denominator stands for the total time during which the excitations were within the membrane.

References

- [1] Scheuring S and Sturgis J 2005 *Science* **309** 484
- [2] Johnson F S 1970 *Biological Conservation* **2** 83
- [3] Janzen H H 2004 *Agriculture, ecosystems and environment* **104** 399
- [4] Knox R S 1977. *Primary Processes of Photosynthesis*, Elsevier-North Holland, p 55
- [5] Pullerits T and Sundstrom V 1996 *Acc. Chem. Res* **29** 381
- [6] Flemming G R and van Grondelle R 1997 *Curr. Opin. Struct. Biol.* **7** 738
- [7] Pfenning N 1978 *The Photosynthetic Bacteria* (New York: Plenum Publishing Corporation) p 3
- [8] Fassioli F, Olaya-Castro A, Scheuring S, Sturgis J N and Johnson N F 2009 *Biophysical Jour.* **97** 2464
- [9] Jang S, Newton M D and Silbey R J (2004) *Phys. Rev. Lett.* **92** 218301
- [10] Scheuring S, Rigaud J L and Sturgis J N 2004 *EMBO* **23** 4127
- [11] Francke C and Ames J 1995 *Photosynthetic Res.* **46** 347
- [12] Geyer T and Heims V 2006 *Biophys. J.* **91** 927
- [13] Bahatyrova S, Freese R N, Siebert C A, Olsen J D, van der Werf K O, van Grondelle R, Niederman R A, Bullough O A, Otto C and Hunter N C 2004 *Nature* **430** 1058
- [14] Hu X, Ritz T, Damjanovic A, Autenrieth F, and Schulten K 2002 *Quart. Rev. of Biophys.* **35** 1
- [15] Lee H, Cheng Y, and Flemming G 2007 *Science* **316** 1462
- [16] Engel G S, Calhoun T R, Read E L, Ahn T, Mancal T, Cheng Y, Blankenship R, Fleming G R 2007 *Nature* **446** 782
- [17] Hess S, Chachisvilis M, Timpmann K, M. Jones, G. Fowler, C. Hunter, and V. Sundstrom 1995 *Proc. Natl Acad. Sci. USA* **92** 12333
- [18] Ritz T, Park S and Schulten K 2001 *J. Phys. Chem. B* **105** 8259
- [19] Damjanovic A, Ritz T, and Schulten K 2000 *Int. J. Quantum Chem.* **77** 139
- [20] Bergstrom H, van Grondelle R, and Sundstrom V 1989 *FEBS Lett.* **250** 503
- [21] Visscher K, Bergstrom H, Sundstrom V, Hunter N. C. and van Grondelle R 1989 *Photosyn. Res.* **22** 211
- [22] van Grondelle R, Dekker J, Gillbro T, and Sundstrom V 1994 *Biochim. Biophys. Acta* **1187** 1
- [23] Timpmann K, Zhang F, Freiberg A and Sundstrom V 1993 *Biochim. Biophys. Acta* **1183** 185
- [24] Savoth O and Maroti P 1997, *Biophys. J.* **73** 972
- [25] Milano F 2003 *Eur. Journ. Biochem* **270** 4595
- [26] Caycedo-Soler F, Rodríguez F J, Quiroga L and Johnson N F (2010) *Phys. Rev. Lett* **104** 158302
- [27] Schuring S and Sturgis J N 2006 *Biophys. Jour.* **91** 3707
- [28] Scheuring S, Sturgis J N, Prima V, Bernadac A, Lévi D and Rigaud J L 2004 *Proc. Natl Acad. Sci. USA* **101** 11293

- [29] Liu L, Duquesne K, Sturgis J N and Scheuring S 2009 *J. Mol. Biol.* **393** 27
- [30] Caruso F, Chin A W, Datta A, Huelga S F and Plenio M B 2009 *J. Chem. Phys.* **131** 105106
- [31] Plenio M B and Huelga S F 2008, *New J. Phys.* **10** 113019